Meteorologische Zeitschrift, Vol. **12**, No. 3, 143-156 (June 2003)

Article

Ice supersaturation in the tropopause region over Lindenberg, Germany

PETER SPICHTINGER[1,*], KLAUS GIERENS[1], ULRICH LEITERER[2] and HORST DIER[2]

[1] Deutsches Zentrum für Luft- und Raumfahrt, Institut für Physik der Atmosphäre, Oberpfaffenhofen, Germany
[2] Deutscher Wetterdienst, Meteorologisches Observatorium Lindenberg, Germany

(Manuscript received January 22, 2002; in revised form February 6, 2003; accepted April 13, 2003)

Abstract

The occurrence of ice-supersaturation layers (in either clear air or in cirrus) over the Meteorological Observatory Lindenberg is investigated for the period February 2000 to April 2001 by means of the humidity, temperature, and pressure reports obtained from the Lindenberg corrected RS80A routine radiosonde. The RS80A routine sonde data are corrected on the basis of weekly comparison ascents with Lindenberg research radiosonde humidity data. This research sonde applies the Lindenberg measuring and evaluation technique of "standardized frequencies". We study the frequency of occurrence of ice supersaturation in the tropopause region over Lindenberg, the vertical distribution of ice-supersaturation layers in the upper troposphere and lowermost stratosphere, their situation relative to the tropopause, their vertical dimensions, their temperatures and the statistical distribution of relative humidities. The mean frequency of occurrence of ice-supersaturation layers is about 28%. Most of them occur within a broad layer extending 200 hPa down from the tropopause. Most events occur in cold air with temperature below $-40°$C. Their vertical extensions can be fitted by a pair of Weibull distributions with mean 560 ± 610 m. The results are compared with findings from the MOZAIC project, from the SAGE II satellite instrument, and with various results from Lidar measurements.

Zusammenfassung

Korrigierte Routine-Radiosondendaten der Sonde RS80A (Feuchte, Temperatur, und Druck) werden hinsichtlich des Auftretens von Eisübersättigung (in klarer Atmosphäre sowie in Zirren) über Lindenberg für den Zeitraum Februar 2000 bis April 2001 ausgewertet. Die Korrektur erfolgt anhand wöchentlicher Vergleichsaufstiege mit der Forschungssonde des Meteorologischen Observatoriums Lindenberg. Die Forschungssonde nutzt das Lindenberger Mess- und Auswerteverfahren der "standardisierten Feuchtefrequenzen". Wir untersuchen die Häufigkeit des Auftretens von Eisübersättigung über Lindenberg, die Höhenverteilung der Schichten, in denen Eisübersättigung auftritt, in der oberen Troposphäre und untersten Stratosphäre, deren Lage relativ zur Tropopause, deren vertikale Mächtigkeit, deren Temperaturen, sowie die statistische Verteilung der relativen Feuchte. Im Mittel kommt Eisübersättigung in etwa 28% der Sondenaufstiege vor, meistens in einem Bereich bis zu 200 hPa unterhalb der Tropopause, und die Temperatur liegt meistens unterhalb -40 °C in den eisübersättigten Luftmassen. Die Verteilung der vertikalen Ausdehnung der eisübersättigten Luftmassen lässt sich durch ein Paar von Weibull-Verteilungen anpassen, wobei die mittlere vertikale Ausdehnung etwa 560 ± 610 m beträgt. Die Ergebnisse werden mit Resultaten des MOZAIC-Projektes und des SAGE II Satelliteninstrumentes verglichen, sowie mit diversen von Lidarmessungen gewonnenen Ergebnissen.

1 Introduction

Cirrus clouds in the cold tropopause region are believed to form mainly by homogeneous freezing of aqueous solution droplets (cf. HEYMSFIELD and MILOSHEVICH, 1993; HEYMSFIELD and SABIN, 1989; SASSEN and DODD, 1988). At temperatures lower than $-40°$C this process requires airmasses in a state of substantial supersaturation with respect to ice (generally more than 40%, KOOP et al., 2000). Such a high supersaturation can be achieved by either cooling of airmass, by water advection, or by appropriate mixing of two airmasses (as in formation of condensation trails). However, an airmass that once reaches ice supersaturation does not necessarily later reach the freezing threshold and thus there exist airmasses that are supersaturated but clear. Such regions have been termed **i**ce-**s**upersaturated **r**egion**s** (**ISSRs**, GIERENS et al., 1999). Evidently, an airmass containing a cirrus cloud must have gone through an ISSR stage. Further, it is possible that a thin or subvisible cirrus occurs as a transient phenomenon in an ISSR, when ice crystals sediment out of the region while the region itself remains in an uplifting state.

ISSRs have been detected by a variety of hygrometers during several airborne measurement campaigns. The types of instruments include frost point hygrometer (OVARLEZ et al., 2000), tunable diode laser (JENSEN et al., 1998; VAY et al., 2000), and the capacitive sen-

* Corresponding author: Peter Spichtinger, DLR Institut für Physik der Atmosphäre, Oberpfaffenhofen, D-82234 Weßling, Germany, e-mail: peter.spichtinger@dlr.de

0941-2948/03/0012-0143 $ 06.30
DOI: 10.1127/0941-2948/2003/0012-0143

sor (HELTEN et al., 1998, 1999). The latter is installed on five commercial aircraft within the **M**easurement of **oz**one by **A**irbus **i**n-service air**c**raft (**MOZAIC**) project (MARENCO et al., 1998). The MOZAIC data were used by GIERENS et al. (1999) to determine the frequency of occurrence of ISSRs over the northern midlatitudes and to determine the statistics of relative humidity within ISSRs. Mean temperature differences of 3–4 K between ISSRs and their subsaturated environment (ISSRs are colder) could be determined in the same work as well as water vapour mixing ratios in ISSRs that exceed their counterparts in the neighbouring subsaturated regions by typically a factor 1.5. GIERENS et al. (2000) related the MOZAIC data to statistics of occurrence of subvisible cirrus clouds (WANG et al., 1996), obtained from data of the **S**tratospheric **A**erosol and **G**as **E**xperiment **II** (**SAGE II**) on board the **E**arth **R**adiation **B**udget **S**atellite (**ERBS**). A close relation between ISSRs and subvisible cirrus is probable according to that work. Typical horizontal extensions of ISSRs could be determined from the MOZAIC data by GIERENS and SPICHTINGER (2000). Recently, data from the **M**icrowave **L**imb **S**ounder (**MLS**) on board the **U**pper **A**tmospheric **R**esearch **S**atellite (**UARS**) were evaluated by SPICHTINGER et al. (2002) in order to obtain a global version of the humidity statistics inside and outside ISSRs.

Radiosondes are not included in the above list of instruments used for measuring humidity in ISSRs. The reason for this is that hygrometers that are operational in current radiosonde types (usually RS80 with A-Humicap by Vaisala) cease to furnish reliable results in cold air ($T < -40°C$) or at low absolute humidities, conditions that are typical for the upper troposphere and beyond (e.g. NASH and SCHMIDLIN, 1987; ELLIOTT and GAFFEN, 1991). However, the situation is beginning to improve with the advent of the new H-Humicap sensor of Vaisala and the RS90 sonde (ANTIKAINEN and JAUHIAINEN, 1995). The Lindenberg Observatory of Deutscher Wetterdienst has developed the method of "standardized frequencies" (LEITERER et al., 1997), so-called FN-method, using a modified RS90 as a research radiosonde. This method allows to obtain very accurate relative humidities using the research sonde throughout the troposphere and into the lowermost stratosphere. The research sonde has been used to correct the routine RS80 A radiosondes (LEITERER et al., 2002[1]; NAGEL et al., 2001). Hence, this data can be used to examine the upper troposphere and lowermost stratosphere concerning relative humidity with respect to ice.

As radiosonde reports do not contain any information about the concentration of ice crystals along their path, it is not possible to distinguish between cloudy and cloud-free parts of a profile. However, evaluating the Lindenberg data we find certain signatures that are characteristic of ISSRs and others that are characteristic of cirrus clouds (see below, in particular 3.4 and 3.5). Further, radiosondes of good quality can be used to study the vertical extension of ice supersaturated airmasses (ISSR and cirrus) and their situation relative to the local tropopause. Such investigations are the topic of the present paper.

In the next section, the FN-method for the research sonde and the method for correction of the RS80 A-Humicap profiles (the Lindenberg routine radiosonde 4 times daily) will be described. Section 3 then presents and discusses the results. These are summarised, and conclusions are drawn in Section 4.

2 The Lindenberg corrected RS80 A data

2.1 Fundamental principles of calibration and corrected RS80 A humidity profiles

Weekly comparison ascents of the routine RS80 A-Humicap radiosonde with the Lindenberg research radiosonde (a modified type of the RS90 radiosonde) are the basis of the calibration. The research radiosonde uses the Lindenberg measuring and evaluation method of "standardized frequencies" (**FN-method**) (LEITERER et al., 1997) as described in Section 2.1.1. The derived correction procedure for RS80 A-Humicap data is described in Section 2.1.2.

2.1.1 The FN-method

A new measuring and evaluation method has been developed at the Meteorological Observatory Lindenberg which is suited for using the modified RS90 sensor unit as reference humidity sensor during the radiosonde ascent. The general measuring technique is based on the capacity dependence of a thin polymer layer in relation to the quantity of water molecules which are oozed into the polymer structure. The capacity will be transformed into frequencies by a resonant circuit of the radiosonde transmitter. The technical improvements of the RS90 sensor unit with reference to the RS80A sensor unit are described in detail by Vaisala authors (ANTIKAINEN and PAUKKUNEN, 1994; PAUKKUNEN, 1995; ANTIKAINEN and JAUHIAINEN, 1995). Both polymer sensors measure the partial pressure relation $\frac{e_w}{e_{sw}}$ (e_w: partial pressure of water vapour; e_{sw}: saturation partial pressure of water vapour over plane liquid water surface) or the relative humidity with respect to water even under water or ice saturated and supersaturated conditions (in ISSR and cirrus) as reported in NAGEL et al., 2001.

The FN-method of "standardized frequencies", described in detail in a series of publications (LEITERER et al., 1997; LEITERER et al., 2002; NAGEL et al., 2001), enables us to carry out reference humidity soundings in comparison to other humidity soundings. The absolute accuracy of the new measuring and evaluation technique is about $\pm 1\%$ RH in the temperature

[1] aviable from: www.dwd.de/de/FundE/Observator/MOL/mol3/mol3_RS80_kor.pdf

Table 1: Coefficients for the polynomials of the calibration matrix in Fig. 1, as functions of the standardised frequencies FN.

$$U(t) = A(FN) \cdot t^2 - B(FN) \cdot t + C(FN)$$

FN	$A(FN)$	$B(FN)$	$C(FN)$
0.0	0.0008	0.0384	0.4867
0.1	0.0013	0.0809	6.859
0.2	0.0014	0.1426	16.116
0.3	0.002	0.1605	25.509
0.4	0.0023	0.1721	36.362
0.5	0.0029	0.1407	46.719
0.6	0.0027	0.1176	58.186
0.7	0.0025	0.0986	69.797
0.8	0.0023	0.0974	81.393
0.9	0.0025	0.1109	91.159
1.0	0.0027	0.0982	100.55

region of 35 to −70°C. The sensor unit consists of the F-Thermocap (for temperature) and two alternately heated H-Humicaps (for relative humidity, RH) which are heated during 60 s and are used for measurement during 160 s. The measuring frequencies, if heating is switched on, are used as additional calibration points at 0% RH during the radiosonde ascent. Therefore one receives alternate data from both humidity sensors which make up one humidity profile. The absolute calibration (standardization) is derived from a so-called ground-check using a calibration box ventilated with 5 m/s at saturation-conditions (100% RH) and room temperature (20 to 25°C). The individual difference ΔF (in the order of 200.0 Hz) will be measured for each Humicap with an accuracy of 0.1 Hz a few minutes before the ascent, with $\Delta F = F_H - F_{M,100}$ (F_H = measuring frequency of heated Humicap at 100% RH; $F_{M,100}$ = measuring frequency of unheated Humicaps at 100% RH). On the basis of this frequency difference ΔF, the so-called individual standardized frequencies FN_i for each measuring point i (every 1.6 s) during an ascent will be calculated with:

$$FN_i = \frac{\bar{F}_{Hi} - F_{Mi}}{\Delta F} \tag{2.1}$$

with

$\bar{F}_{Hi}$: individual mean frequency of heated sensor during the heated cycle (60 s) equivalent about to 0% RH,

F_{Mi} : individual measuring frequency for each measuring point i (each 1.6 s) during the measuring cycle (160 s).

The evaluation algorithm calculates the exact individual RH, $U_i(\%)$, for each measuring point i using these individual standardized frequencies FN_i on the basis of a FN_i universal calibration matrix (see Tab. 1, Fig. 1). The universal calibration matrix gives the mathematical relation between the standardized frequency FN, the RH, $U(\%)$, with respect to water and temperature t (°C). The absolute accuracy of the sonde is 1% in RH (NAGEL et al., 2001).

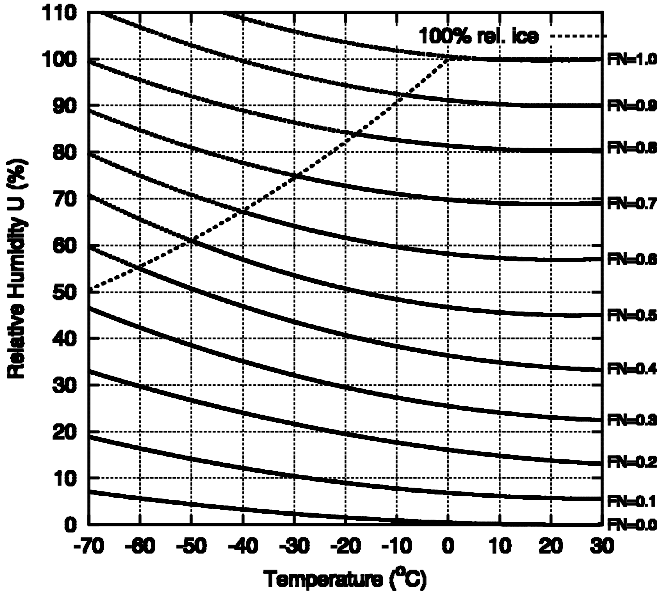

Figure 1: The standardised frequencies FN calibration matrix: The relative humidity U (%) with respect to water as a function of standardized frequencies FN (solid and dotted polynomial curves,labelled with their respective FN) and temperature t. The dashed curve represent the saturation with respect to ice.

2.1.2 The RS80 A-Humicap correction

It is worth mentioning that the RS80 A-Humicap sensor is a polymer humidity sensor which is covered with a rain protection cap. Therefore the ventilation of the humidity sensor is not guaranteed. Icing effects on the sensors occur in about 15 percent of cloudy weather conditions in spite of the rain protection cap (results of 360 especially investigated soundings in Lindenberg). But this partly or total sensor icing is not recognized in routine operation. This means that the uncertainty (standard deviation) of the RS80 A-Humicap humidity data increases.

A special method to recognize icing cases was developed for the Lindenberg station 10393. This method uses climatological water vapour mixing ratio data of about 4.5 ppmv in the lower stratosphere in a height of 5 km above the tropopause (for Lindenberg about 16 km). If the RH data (expressed in ppmv) in the lower stratosphere are higher than a threshold (obtained from research and routine RS80 sondes comparisons) the operator recognizes this case and cancels all RH data in the troposphere with temperatures lower than −10°C.

Despite of this "icing recognition" and elimination of "iced" RH data one has to apply the following correction formula, containing a so-called additional RH ground-check-correction and an additional RH temperature dependent correction (details are described in LEITERER et al., 2002).

$$U_{corr,w} = U_{ms,w} + \left[(U_{psy} - U_{ms,0}) \cdot \frac{U_{ms,w}}{U_{psy}}\right] + \left[0.005 \cdot t^2 + 0.112 \cdot t + 0.404\right] \cdot \frac{U_{ms,w} + (U_{psy} - U_{ms,0}) \cdot \frac{U_{ms,w}}{U_{psy}}}{U_w(t, 100\%\ ice) - (0.005 \cdot t^2 + 0.112 \cdot t + 0.404)} \quad (2.2)$$

Eq. 2.2 has been applied at the station 10393 (Lindenberg) since January 2000.
$U_{corr,w}$ is the corrected RS80 RH with respect to water.
$U_{ms,w}$ denotes the measured RS80 RH (with respect to water) corresponding to Vaisala factory calibration and the dry ground-check (with 0% RH corresponding to the instructions for use).
U_{psy} stands for measured RH by the psychrometer in the weather screen before the ascent and
$U_{ms,0}$ is the measured RH by the RS80 in the weather screen before the ascent.
t is the temperature in degree Celsius (°C).

$$U_w(t, 100\%\ ice) = \frac{e_{si}(T)}{e_{sw}(T)} \cdot 100\% \quad (2.3)$$

stands for the computed RH with respect to water at the actual temperature t and ice saturation.
e_{si} and e_{sw} are the saturation partial pressure of water vapour at the temperature T over plane ice or liquid water, respectively. The saturation curves are taken from SONNTAG (1994).
$T = 273.16\ \mathrm{K} + t$ is the temperature in Kelvin (K).

The quality of humidity standard aerological soundings has been improved essentially in recent years applying these additional corrections to the data produced by Vaisala standard product software.

Fig. 2 shows the improved quality of the corrected RS 80 A-Humicap soundings derived from synchronized soundings RS80 A-Humicap and Lindenberg research reference sonde in the period July 1999 until September 2000 at Lindenberg 10393 upper air station. For the upper troposphere the dry bias (dotted line) of about −8% RH near 300 hPa is nearly completely eliminated (thick line). Only a small dry bias of maximum 3 % remains in the boundary layer between 1000 and 850 hPa. In higher levels the bias is smaller than 0.5% relative humidity and in the investigated region of 600–100 hPa the mean bias is about −0.3% RH, the mean standard deviation is about 1.9% RH. We hope that the remaining dry bias can also be removed, but the research is going on regarding this subject.

2.2 Data selection

For the present study we use the Lindenberg corrected RS80A data for the period February 1, 2000 until April 30, 2001. There are usually four ascents per day, at 00, 06, 12, and 18 UTC, respectively. From these ascents we obtain profiles of pressure, temperature and relative humidity with respect to liquid water. The reported values are 10 s averages and cover a pressure range from surface pressure to about 100 hPa. Additionally we use tropopause pressure and altitude. From the total of 1666 ascents we had to dismiss 103, because of missing data or other problems, so we have data from 1563 ascents for evaluation.

Since we are interested in ice supersaturation in the upper troposphere we evaluate only data for pressure levels above 600 hPa. This seems a rather low altitude for the upper troposphere, yet the lowest pressure altitude of the tropopause in the dataset is 482.7 hPa. The relative humidity with respect to ice, RHi, is computed from $U_{corr,w}$ according to

$$RHi = U_{corr,w} \frac{e_{sw}(T)}{e_{si}(T)} \quad (2.4)$$

A radiosonde crossing a supercooled water cloud reports $RH \approx 100\%$, which would imply ice supersaturation. Yet, this is neither an ISSR nor a cirrus, hence we use a temperature criterion to avoid to count such events. This is, we only register an event when its bottom temperature is lower than −30°C and when simultaneously its top temperature is lower than −35°C. In the range lower than −30°C cloud particles in liquid phase are very seldom (see PRUPPACHER and KLETT, 1997, chap. 7).

3 Results and discussion

3.1 Frequency of ice supersaturation

In the following we often use the term *ice-supersaturation layer* or something similar to denote those parts of the radiosonde profiles where $RHi > 100\%$.

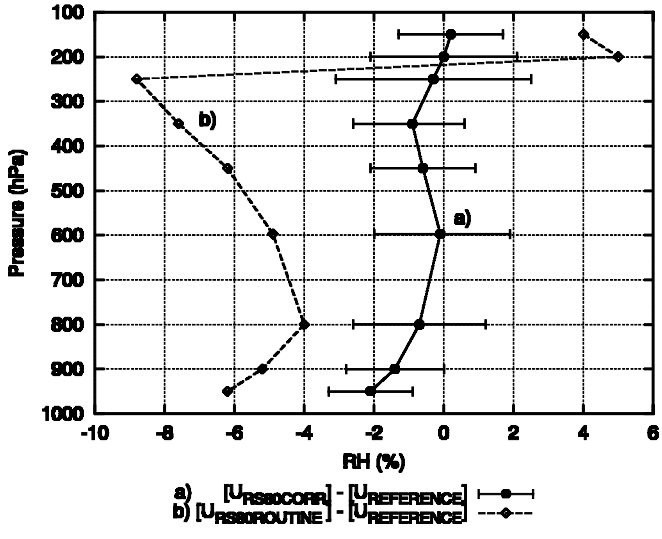

Figure 2: a) Mean differences of relative humidities between corrected RS80 A-Humicap [$U_{RS80CORR}$] and research reference method[$U_{REFERENCE}$] derived from about 70 synchronized soundings RS80 A and Lindenberg research reference sonde (modified RS90) in the period July 1999 till September 2000 in Lindenberg. b) Mean difference of relative humidities between routine radiosonde RS80 A [$U_{RS80ROUTINE}$] and research reference method [$U_{REFERENCE}$], approximate data.

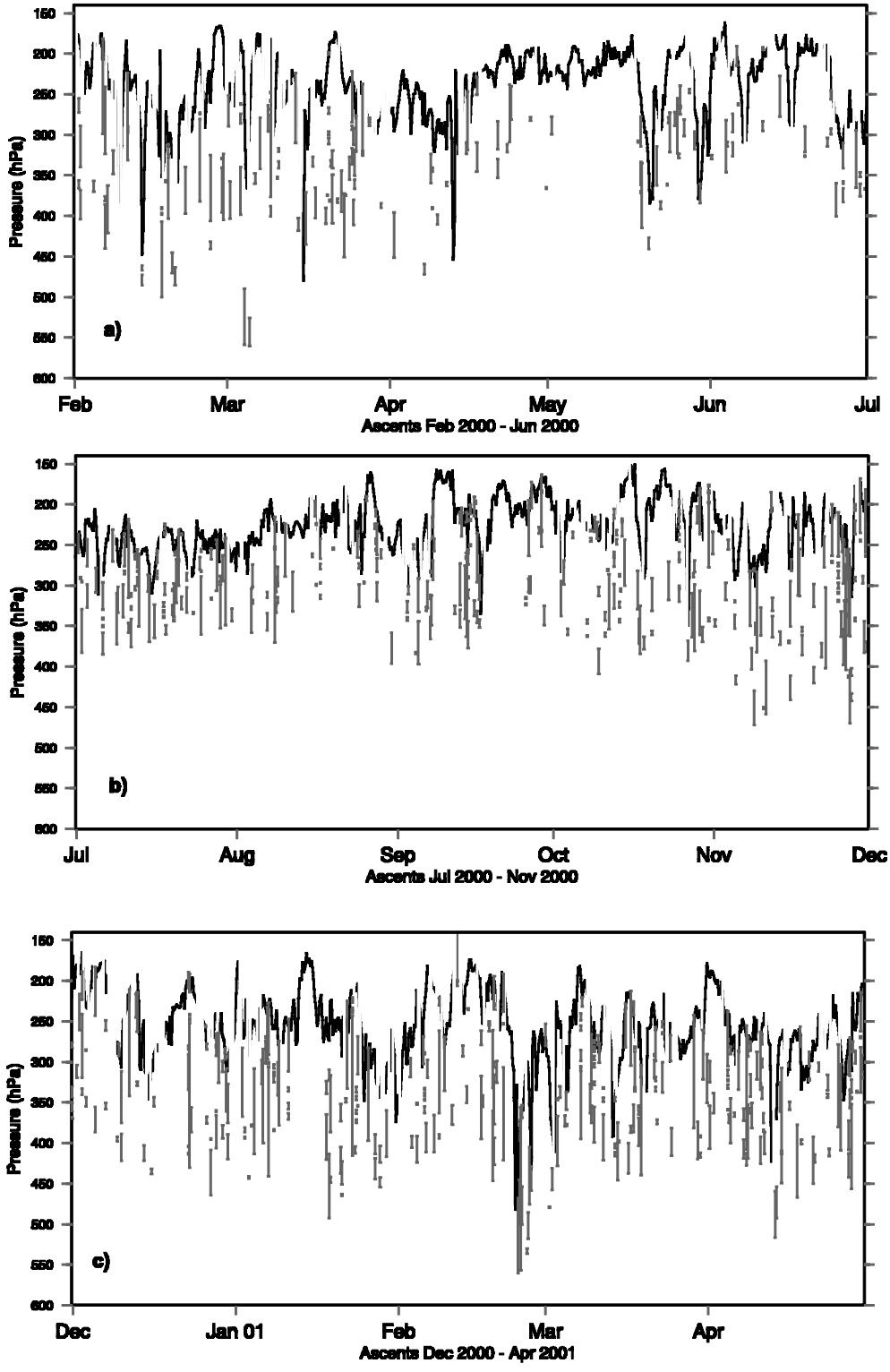

Figure 3: Ice-supersaturation layers over the meteorological station Lindenberg vs. date. The vertical extension of each event is marked by a gray bar. Often there are several layers found within one radiosonde ascent. The tropopause pressure is also given (black line).

Thus, the notion ice-supersaturation layer includes both ice-supersaturated regions (clear air) and cirrus clouds.

Employing the pressure and the temperature criteria we find a total of 730 layers with ice supersaturation (i.e. cirrus and / or ISSRs) in 437 out of the 1563 ascents. Thus, we find ice supersaturation in 28% of the ascents, and often there are more than one ice-supersaturation layer in one ascent. If we allow for a 1.9% *RH* error and a bias of −0.3% *RH* of the humidity measurements and regard the research radiosonde (FN-method) error of 1% *RH*, the total number of layers with ice supersaturation ranges between 641 and 939, and the number of ascents where *RHi* exceeds 100% at least once ranges between 378 (24%) and 540 (35%).

The cloud atlas of WARREN et al. (1986) shows for the region near Lindenberg average cirrus amounts of 17–23%, and cirrus frequencies of occurrence of 44–49%. The radiosonde, being a point measurement, does not always cross a cirrus or an ISSR when cirrus clouds are around. Thus it is clear that the radiosonde data must yield a smaller frequency of occurrence of ice-supersaturation layers than the surface observations of the total sky. Instead, the radiosonde data can be understood as random sample measurements, and thus their frequencies of occurrence of ice-supersaturation layers can be expected to yield values that resemble the average cirrus amounts from the total sky observations. This is indeed found here, but the values from the radiosonde are slightly larger than those of the cloud atlas, probably because of the additional inclusion of cloud free ISSRs or subvisible cirrus in the radiosonde data set.

The measurements of ice-supersaturation layers for each date are given in Fig. 3. Every such layer is marked by a gray bar representing its vertical extension. Also given on the figure is the pressure of the thermal tropopause (black line), and we see immediately that most ice-supersaturation layers remain below the tropopause in the upper troposphere (see below). The multiple ice-supersaturation layers are often separated by rather thin subsaturated layers. It could be that this reflects the internal (vertical) structure of cirrus and ISSRs where perhaps by turbulent entrainment of drier ambient air subsaturated zones are produced in an overall supersaturated layer.

In Fig. 3 we see extended periods of 1–2 weeks where ice supersaturation did not occur in the atmosphere over Lindenberg and there are other periods where ice supersaturation was frequent. The monthly percentages for February 2000 until April 2001 are shown in Fig. 4. The frequencies of occurrence are defined here as the number of ascents per month (or season) that contain one or more ice-supersaturation layer divided by the total number of ascents during the respective period in question. Multiple ice-supersaturation layers are not counted here as multiple events. Since the data cover only a little more than one year, this figure does not represent climatological values; rather the values represent a snapshot where influences of weather anomalies are apparent. For instance, near minimum frequency of ice supersaturation occurs in May 2000, which month was much warmer and drier relative to climatological means, and in turn the July 2000 was colder and wetter (DWD, 2000), and ice supersaturation was reported much more frequent than in either June or August 2000. The frequency of ice supersaturation measurements in the latter months agree better with our expectation of relatively low summer values, since it is known that the relative humidity in the upper troposphere of the mid-latitudes obtains its lowest mean values during summer (KLEY et al., 2000, cha. 3.3.2). Due to the anomalies in 2000, the expected annual cycle cannot be seen in the monthly data. However, when integrating the seasonal means (spring (MAM) 27%, summer (JJA) 24%, fall (SON) 34%, and winter (DJF) 27%) a seasonal cycle similar to that of KLEY et al. 2000 – though not significant – might become visible.

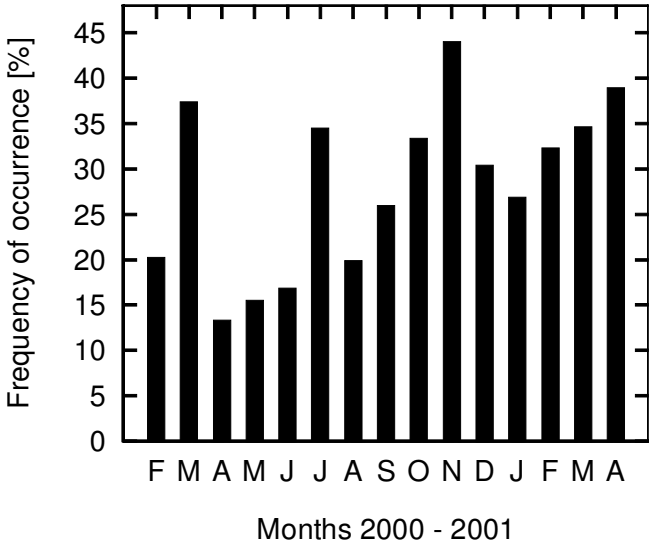

Figure 4: Monthly frequencies of occurrence in percentage of ascents with one or more ice-supersaturation layer over Lindenberg for the period February 2000 until April 2001.

3.2 Altitude distribution of ice-supersaturation layers

Evaluating the data shown in Fig. 3 we can obtain an altitude distribution of ice-supersaturation layers. For this purpose we count the appearance of data with $RHi > 100\%$ on pressure levels from 150 to 600 hPa in steps of 50 hPa, where each level actually means the centre of a 50 hPa thick layer. Ice-supersaturation layers

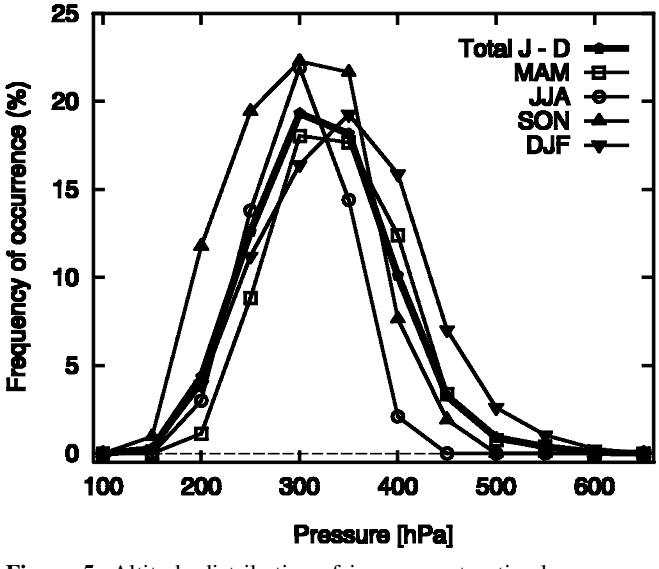

Figure 5: Altitude distribution of ice-supersaturation layers averaged over the whole period (February 2000–April 2001, thick line), and over the seasons (thin lines, see inserted key). Most ISSRs are found in a broad layer between 200 and 450 hPa, with seasonal shifts of the order ±40 hPa.

that extend over more than one layer are counted in each of these layers. The annual mean and seasonal distributions are shown in Fig. 5. The figure shows that ice supersaturation is frequent in a broad upper tropospheric layer between 450 and 200 hPa. In autumn the ice-supersaturation layers reach their highest altitudes, in winter the lowest. The mean altitudes are about 300 hPa in summer and fall, and 340 hPa in winter and spring. This seasonal shift is statistically significant (as a t-test shows), although the distributions are rather broad.

Ice supersaturation is found in 4.4% of the profiles in the 200 hPa layer and in 12.6% of the profiles in the 250 hPa layer in the annual mean. These values vary between 2.4% and 9.0% for the 200 hPa layer and between 10.0% and 17.3% for the 250 hPa layer, respectively, if we allow for measurement errors as mentioned in 3.1.

The annual mean values can be compared with the corresponding values obtained from the humidity evaluations of the MOZAIC project of the years 1995–1997 (GIERENS et al., 2000). These data have been evaluated on a Gaussian grid consisting of 128 cells in zonal direction times 64 cells in the meridional direction, giving a total of 8192 cells of about $2.8° \times 2.8°$. In this grid, Lindenberg (52.22°N, 14.12°E) falls into cell number 1670 ($= 13 \times 128 + 6$). For this cell the probability to find ice supersaturation at 250 ± 25 hPa is 26%. Unfortunately, for the corresponding 200 ± 25 hPa layer there are no MOZAIC data in cell number 1670. The second cell next to but north of Lindenberg is number 1542. There we have ISSR occurrence frequencies of 21% in the 250 ± 25 hPa layer, but only 5% in the 200 ± 25 hPa layer. In the upper considered layer the agreement between the Lindenberg and the MOZAIC data is excellent, but in the 250 hPa layer the Lindenberg data show only about half the values the MOZAIC evaluation gave. We do not currently know the reason for this discrepancy.

In the same way it is possible to compare the occurrence frequencies of ice-supersaturation layers over Lindenberg with the occurrence frequencies of subvisible cirrus clouds obtained from the SAGE II instrument on board ERBS (WANG et al., 1996). The statistics is presented for height levels, since this is the coordinate used in the SAGE II data base. A quick view over Fig. 6 confirms what has been found in an earlier comparison of MOZAIC and SAGE II data, namely that we tend to find subvisible cirrus rather in regions with higher probability of ice supersaturation than in drier regions (GIERENS et al., 2000). This is plausible. However, in the figure we see also that the subvisible cirrus covers a larger altitude range than the ice-supersaturation layers measured over Lindenberg. We believe that this is not really true and that this discrepancy originates from the low horizontal resolution of the SAGE II data, namely 24° longitude × 10° latitude. Lindenberg is only one point in the huge SAGE II pixel, hence such discrepancies in the data are not a surprise. However, the general similarity between the altitude distributions of subvisible cirrus and the ice-supersaturation layers is pleasant and is furthermore robust against random measurement errors mentioned in 3.1.

3.3 Situation of ice-supersaturation layers relative to the tropopause

In Fig. 3 we could see that ice saturation occurs in most cases below the tropopause, even in meteorological situations where the tropopause pressure is relatively high, e.g. in February 2001. In this section we want to study the altitude of the ice-supersaturation layers relative to the tropopause. In case of multiple tropopauses we relate such events to the lowest tropopause.

The situation of ice-supersaturation layers relative to the local tropopause is shown in Fig. 7. The result is unambiguous: Most layers where the humidity exceeds ice saturation remain beneath the tropopause and only a minor fraction of them (13.3%) extend beyond the tropopause into the lowermost stratosphere. Only 6.2% of the ascents report ice supersaturation in the lowermost stratosphere. This is consistent with the statistics of ice supersaturation obtained from MOZAIC data (GIERENS et al., 1999): Only 2% of the measurements obtained on MOZAIC flights in the lowermost stratosphere indicated supersaturation.

Fig. 8 (left part) shows the altitude distribution of the ice-supersaturation layer tops and bottoms relative to the tropopause. For this investigation the layer top and bottom pressures minus the corresponding tropopause pressure are counted in 5 hPa wide pressure bins, and the number of events in each bin are shown in the figure. There is a sharp spike in the curve for the top pressures just above[2] the tropopause, but the integral under this spike is rather small compared to the integral number of ice-supersaturation events that remain completely beneath the tropopause. The figure shows that most cirrus clouds and ISSRs are situated in a broad layer extending 200 hPa down from the tropopause. A similar investigation was carried out by GOLDFARB et al. (2001) for the altitudes of cirrus cloud tops relative to the tropopause at the Observatoire de Haute Provence using Lidar data. Their figure 4 shows most cloud tops at the tropopause (corresponding to our spike in Fig. 8). The clouds prefer the upper troposphere region between tropopause and 2.5 km beneath, and only a smaller fraction of the cloud tops reach into the lowermost stratosphere. Overall there is a strong similarity between the cloud top altitude distribution relative to the tropopause given by GOLDFARB et al. (2001) and the corresponding altitude distribution of ice-supersaturation layers at Lindenberg. In Fig. 5 a seasonal variation of the altitude distribution is apparent. This is clarified in the right panel of Fig. 8, where we

[2] This spike about 5 hPa above the tropopause is probably caused by the temperature dependent lag error of the RS80 A-Humicap. First evaluation shows the necessity to shift this spike about 10 hPa higher so that the spike would actually be about 5 hPa below the tropopause. The final lag correction for RS80 A-Humicap is subject of research of the Lindenberg research team.

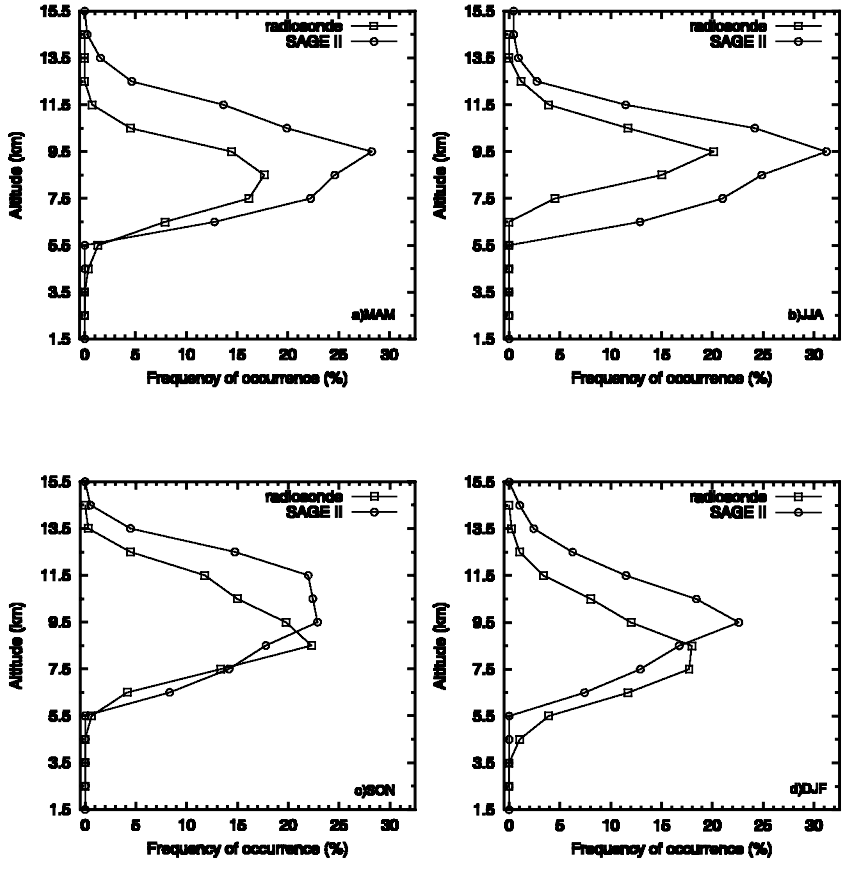

Figure 6: Altitude distribution of ice-supersaturation layers averaged over the whole period (February 2000–April 2001) and frequency of occurrence of subvisible cirrus cloud vs. altitude, as obtained from SAGE II (Wang et al., 1996). The four panels represent a) spring, b) summer, c) autumn, and d) winter.

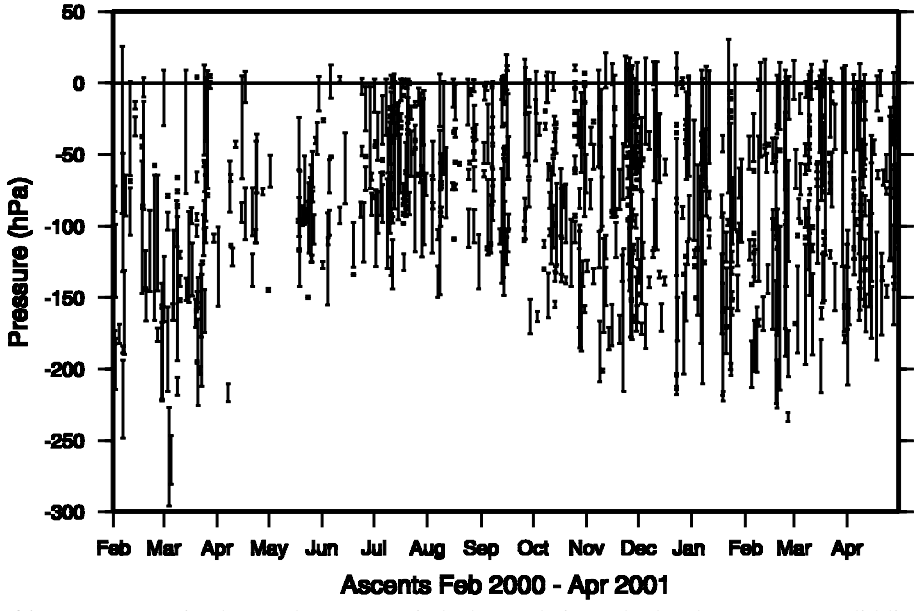

Figure 7: Situation of ice-supersaturation layers (bars) over Lindenberg relativ to the local tropopause (solid line, in case of multiple tropopauses this is the lowest one). The picture is unambiguous: Most events stay below the tropopause and only a minor fraction extends beyond the tropopause into the lowermost stratosphere.

show the seasonal altitude distributions relative to the tropopause (thin lines) together with the annual mean (thick line) expressed as frequency of occurrence (i.e. number of ascents with $RHi > 100\%$ at the considered pressure level divided by the total number of ascents during the considered period). The mean pressure distances from the tropopause are (1 standard deviation in brackets): −92 (58) for spring, −59 (39) for summer, −75

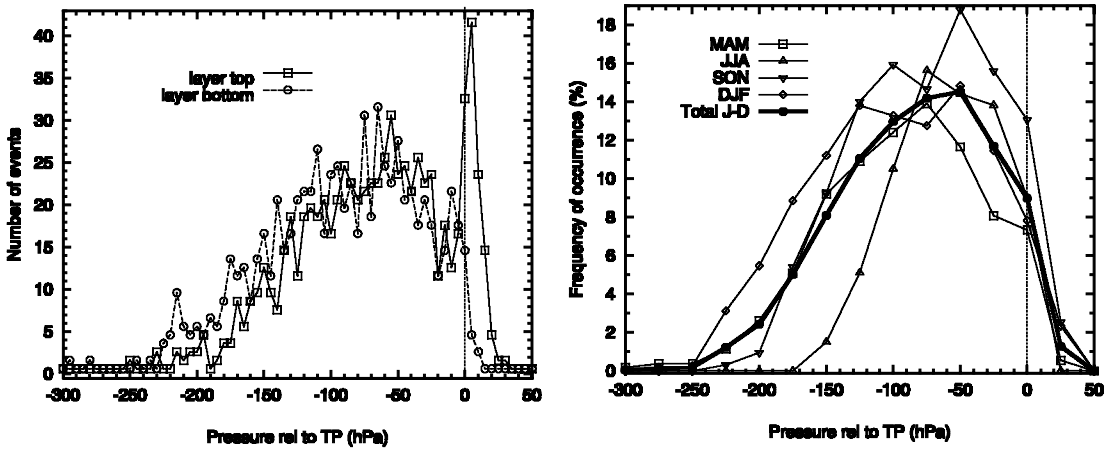

Figure 8: Left panel: situation of ice-supersaturation relative to the tropopause, expressed as pressure of layer top (open squares) and bottom (open circles) minus tropopause pressure. The numbers of events are counted in 5 hPa wide pressure bins. Right panel: Seasonal variation of the situation of ice-supersaturation relative to the tropopause. The thick line is the average over the whole period, while the thin lines are seasonal averages (see inserted key).

(54) for fall, −96 (63) for winter, and −84 (58) for the whole year (all in units of hPa). There is a clear summer vs. rest-of-the-year difference both in the relative altitude of the ice-supersaturation layers as well as in the depth of the atmospheric layer which contains cirrus and ISSRs. The layer where cirrus and ISSRs are found is considerably shallower in summer than in all other seasons and the cirrus clouds and ISSRs are on average nearer to the tropopause in summer than during the rest of the year. A t-test proofs that the summer distribution is significantly different from all other seasonal distributions and this statement remains valid if we allow for the errors in humidity measurements mentioned in 3.1.

3.4 Vertical extension of ice-supersaturation layers

The horizontal scale of cirrus clouds can cover some orders of magnitude. DOWLING and RADKE (1990) estimate a typical scale of 20–30 km, but they say that maximum and minimum extents can be larger or smaller than this by two orders of magnitude. The horizontal scale of ISSRs is well known neither. GIERENS and SPICHTINGER (2000) estimated a typical horizontal width of about 150 km, and found that there are sometimes rather extended ISSRs (up to more than 3000 km). These sizes have been inferred from the MOZAIC data, and it has been stated that as a consequence of a severe selection bias in the data it cannot be excluded that most ISSRs have a much smaller horizontal extension of the order of only a few km. Such a size would agree with horizontal extensions of subvisible cirrus clouds measured with Lidars at Table Mountain (California, see BEYERLE et al., 2001). The MOZAIC data resulting from level flights cannot be used to infer the vertical extension of ISSRs. But the corrected RS80A data can be used to explore the distribution of the vertical extents of ice-supersaturation layers.

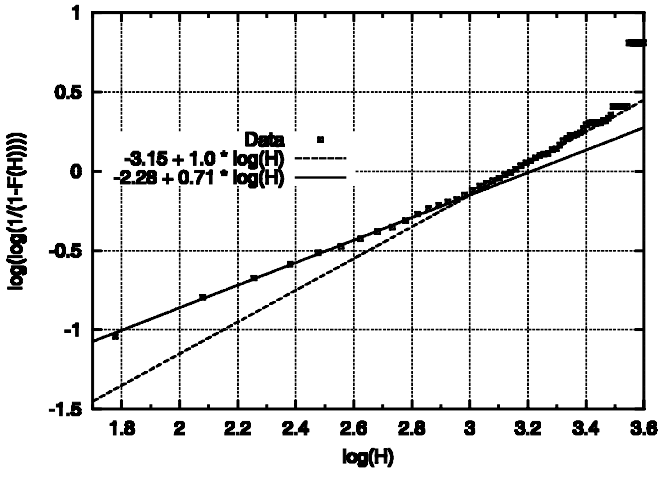

Figure 9: Weibull-plot of the cumulative frequency distribution $F(H)$ of the vertical extension H (in metres) of ice-supersaturation layers (open squares) and two distinct Weibull distribution fits (solid and broken line).

The statistical distribution of vertical extension, H, of ice-supersaturation layers is plotted in Fig. 9 on a so-called Weibull plot. In order to produce this plot the data have been binned into 60 m wide classes for noise reduction, then the cumulative frequency distribution $F(H) = 1 - \exp(-\gamma H^p)$ with shape parameter p and scale parameter γ has been calculated and $\log\log\{1/[1-F(H)]\}$ has been plotted vs. $\log H$. This way of data presentation has the advantage that a Weibull distribution appears as a straight line with slope p. The scale parameter γ can be computed from the intercept q via $\gamma = 10^{q+m}$ with $m = -\log\log(e) = 0.362215\ldots$. Fig. 9 shows that the thicknesses of ice-supersaturation layers indeed seem to follow a Weibull distribution, however with different slopes for shallow and thick layers. The transition between these regimes occurs at a thickness of about 1 km ($\log H = 3$). The slope for the shallower layers is $p = 0.71$, whereas that for the thicker ones is $p = 1$. If we allow for the humidity measurement errors mentioned before the slope for the shallow layer thickness distribution is hardly af-

fected at all while for the thicker ones it varies between 0.9 and 1.1.

The horizontal sizes of ISSRs and cirrus clouds are also Weibull distributed (GIERENS and SPICHTINGER, 2000; BERTON, 2000). The shape parameter is $p = 0.55$ for ISSRs (GIERENS and BRINKOP, 2001). For visible cirrus the corresponding shape parameters are $p = 0.5$ for the horizontal size distribution and $p \approx 1$ for the thickness distribution (BERTON, 2000). The latter result is an indication that the data in our sample with $\log H > 3$ are probably dominated by cirrus clouds, because they follow the same distribution type as in BERTON's sample. For the same reason we believe that the data for $\log H < 3$ in our sample are mostly ISSRs, subvisible cirrus, and perhaps single thin layers of multilayer cirrus clouds. Since there are more data in the $\log H < 3$ branch of our distribution than in the other, the thinner objects dominate the sample, and thick cirrus is only a minor contributor to the data set.

The mean thickness of the ice-supersaturation layers in the radiosonde data is 560 m with a standard deviation of 610 m. Allowing for the errors mentioned in section 3.1 the mean thickness ranges between 490 and 610 m, the standard deviation ranges between 540 and 740 m. This is considerably less than the typical thickness of (visible) cirrus clouds of 1.5 km (DOWLING and RADKE, 1990). Also the mean thickness of cirrus clouds in the statistical sample used by BERTON (2000) is larger (about 3 km, calculated from his tab. 3 using coefficients from section 5.2 and tab. A4). In a most recent compilation of cirrus properties from 10 years of observations (SASSEN, 2002, tab. 2.3) there is not an entry giving cloud thickness of less than 1 km. The mean thickness of the ice-supersaturation layers over Lindenberg is more similar to the thickness of subvisible cirrus clouds that have been measured using Lidars (e.g. SASSEN and CHO, 1992; WINKER and TREPTE, 1998; BEYERLE et al., 2001; GOLDFARB et al., 2001).

3.5 Statistics of relative humidity

The relative humidity field is usually very intricate in space and time since fluctuations of both temperature and absolute humidity are involved in variations of it. However, it turns out that the relative humidity in the tropopause region obeys simple statistical laws over longer periods of time and larger spatial scales. This has been demonstrated using MOZAIC data (GIERENS et al. 1999) and data from the **M**icrowave **L**imb **S**ounder (**MLS**, SPICHTINGER et al. 2002). The statistical laws are: (1) the probability for the relative humidity with respect to ice to reach a certain value in the lowermost stratosphere decreases exponentially with this value, and (2) the probability for the supersaturation with respect to ice, $Si = RHi - 100\%$, to reach a certain value in a tropospheric ISSR decreases exponentially with this value. Expressed by formulae, this reads:

$$P_{RH}(u) = a \exp(-au) \quad \text{(lowermost stratosphere)} \qquad (3.1)$$

$$P_{Si}(s) = b \exp(-bs) \quad \text{(troposph. supersaturation)} \qquad (3.2)$$

where a, b are constants, and u, s are variables on the RH and Si axes, respectively. P means probability density. However, the humidity statistics outside and inside cirrus clouds are fundamentally different: the relative humidity within cirrus clouds turns out to be better described by either a Gaussian or a Rayleigh distribution centred at saturation (OVARLEZ et al., 2002). Now the question arises whether the 15 months of humidity data from the station Lindenberg display a similar statistical behaviour, although they do not cover a large region, and whether both types of humidity distribution (i.e. Gauss/Rayleigh for data obtained in cirrus and exponential for data from clear air ISSRs) are present in the sample. For this evaluation we have used all RHi-data above 600 hPa without any additional temperature

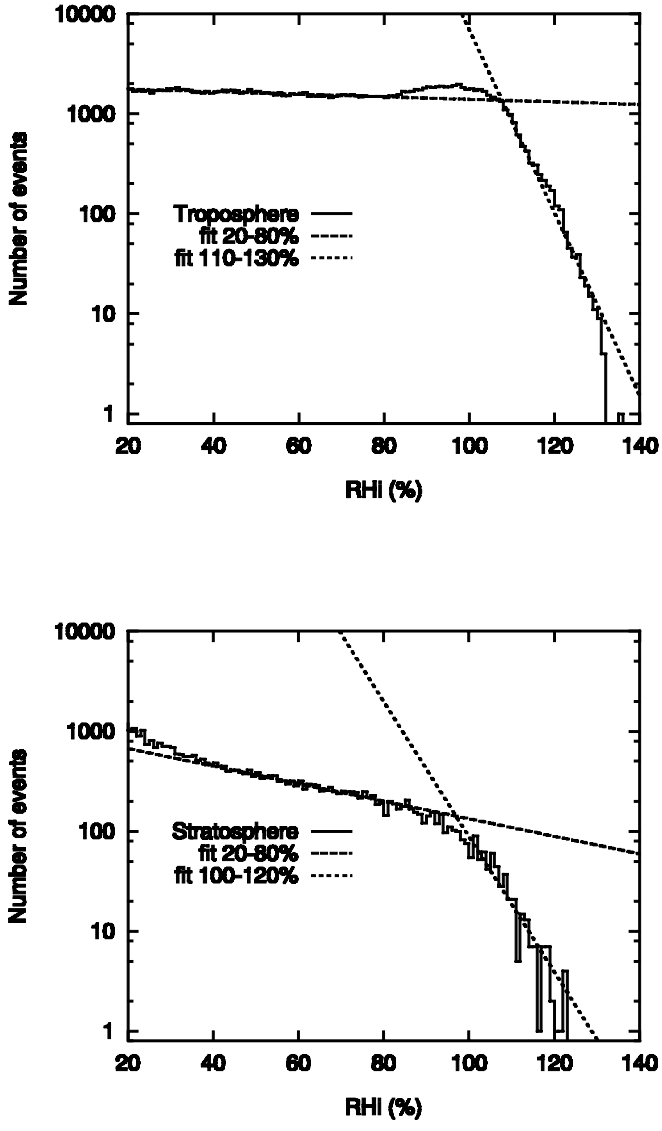

Figure 10: Statistical distribution (non-normalised) of relative humidity with respect to ice, RHi (%), in the troposphere (upper panel) and in the lowermost stratosphere (lower panel) over Lindenberg. Radiosonde data (solid steps) and several exponential fits (broken lines) are presented together.

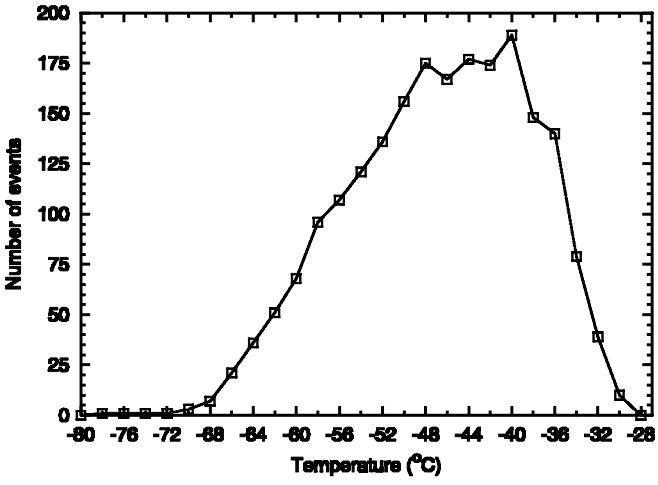

Figure 11: Temperature distribution of ice-supersaturation layers over Lindenberg. The temperature classes are 2 K wide, an event belongs to a temperature class T if at least once the temperature T was measured inside the layer.

criterion. However, there is no change in the shape of the distributions if, for example, we use only data with temperatures lower than $-30°$ C.

Considering first the tropospheric data (Fig. 10, upper panel), we find a statistical distribution of Si resembling that in the earlier study with the MOZAIC data, i.e. a flat distribution for subsaturated values and an exponential distribution for the supersaturated cases. The average supersaturation is $(6 \pm 5)\%$. Additionally, there is a distinct bulge around saturation in the distribution that is the superposition of a noisy Gaussian upon the humidity distribution. Such a bulge is not present in the MLS data and hardly perceivable in the MOZAIC data since these data were cloud cleared as far as possible. Hence, the bulge probably stems from radiosonde measurements inside cirrus clouds. The humidity has relaxed to its equilibrium value (i.e. saturation) in these stable cirrus clouds and merely some fluctuations around saturation remain and lead to the width of the bulge (about 80 to 110%). The exponential distribution of supersaturation above $RHi = 110\%$ is characteristic of ISSRs. However, the slope b of the exponential is much steeper for the Lindenberg data ($b = 0.21$) than in the former studies (MOZAIC: $b = 0.058$; MLS, northern hemisphere: $b = 0.051$). It is not possible to ascribe this difference to vertical variations, since the slope of the exponential is this steep in the Lindenberg data in 8 atmospheric layers, each 50 hPa thick and centred around 500 up to 150 hPa (not shown).

It is more likely that the steep slope in the Lindenberg distribution is caused by the slow response of radiosondes to humidity variations, especially in cold air. In fact, the response time of Vaisala Humicap sensors increases exponentially with decreasing temperature; at $-40°$C the time constant of the RS80A sensor is 27 s (MILOSHEVICH et al., 2001), whereas the data is transmitted every 10 s. The slow response means that sharp maxima in the humidity profile cannot be resolved. The RHi-distributions in the 8 atmospheric layers mentioned above tend to show higher supersaturations in the lower layers and vice versa – consistent with the shorter response time in these relatively warm layers. Although the MOZAIC sensors suffer from a time lag, too, this error source is not as effective as for the radiosonde because a MOZAIC aircraft generally stays in the same altitude for a period much longer than the time constant of the sensors, and the RHi-field has certainly larger autocorrelation scale lengths in the horizontal than in the vertical.

Looking at the stratospheric data (Fig. 10, lower panel), the distribution is different from the earlier distributions of RHi of both MLS and MOZAIC. Instead of getting a constant slope from low humidities (say 20%) up to highly supersaturated values we rather get a distribution that is similar to the aforementioned tropospheric distribution, albeit without the bulge at saturation; in particular there is a kink in the distribution at ice saturation. This kink at saturation signifies physical processes acting on the water vapour reservoir in different ways on the sub- and supersaturated sides, respectively, and it is most plausible to assume that it is the presence of clouds in the supersaturated regime that is responsible for the kink. A straight distribution without a kink at saturation thus indicates cloud free conditions, and that was probably the case in most of the MOZAIC and MLS data assigned to the stratosphere that were evaluated earlier. On the contrary, we must assume that clouds above the thermal troposphere influenced the observed distribution of RHi over Lindenberg. Note that the tropopause definition used for the present evaluation is much sharper than those used for either the MOZAIC data or the MLS data, since we have the exact tropopause pressure available and data immediately above the thermal tropopause can be assigned to the stratosphere. Cirrus and subvisible cirrus above the mid-latitude tropopause have indeed been observed by satellite instruments (e.g. SAGE II, WANG et al., 1996) or by the **C**ryogenic **I**nfrared **S**pectrometers and **T**elescopes for the **A**tmosphere (**CRISTA**, SPANG et al., 2002). Clouds immediately above the tropopause could therefore affect the RHi distribution as observed here. The missing of the bulge around 100% could mean, that these ice clouds in the lowermost stratosphere do rarely relax to equilibrium, and that the ice crystals would fall out of the supersaturated layer before the moisture available for condensation is completely used up for crystal growth.

3.6 Temperature distribution of ice-supersaturation layers

Evaluating the data shown in Fig. 3 we can obtain a temperature distribution for the ice-supersaturation layers. For this purpose we define 26 classes of temperature between $-30°$C and $-80°$C, each class 2 K wide ($k_T = \{T_{meas} | T - 1\text{K} \leq T_{meas} < T + 1\text{K}\}$). An ice-supersaturation layer belongs to a temperature class if at

least once the temperature T has been measured inside the layer. The thicker ones of the ice-supersaturation layers in our data set will normally contribute to more than one temperature class. We obtain a distribution of temperature as shown in Fig. 11. The major part of the measured temperatures is lower than -40°C (in fact 71% of them), the mean value is -46.8°C and the standard deviation is 8.4 K. This general result is only slightly affected by the random errors of humidity measurements: The fraction of events in which the measured temperature is lower than -40°C ranges between 70% and 75%. The shape of the distribution is virtually unaltered; only the mean value and the standard deviation slightly vary between $(-46.4 \pm 8.4)^{\circ}$C and $(-48.0 \pm 8.8)^{\circ}$C.

4 Summary and conclusions

In the present work we have evaluated radiosonde data of the meteorological observatory Lindenberg in order to determine properties of ice-supersaturation layers and statistical properties of the relative humidity in the tropopause region. The term ice-supersaturation layer is here used to designate a measurement of the relative humidity with respect to ice in excess of 100%, irrespective of the presence of ice crystals (since cloud information is not contained in radiosonde profiles). Thus an ice-supersaturation layer can either be a cirrus cloud or an ice-supersaturated region (ISSR), that is a supersaturated but cloud free airmass. The data, taken with a RS80A radiosonde and corrected by means of a research sonde, cover 15 months from February 2000 to April 2001. The following results therefore must not be interpreted in a climatological sense. The main results are:

1. We find a total number of 730 ice-supersaturation layers in 437 of 1563 ascents, hence the mean frequency of occurrence of ice supersaturation over the station Lindenberg for the tested period is about 28% with seasonal fluctuations between 24% (summer) and 34% (fall). These values are consistent but slightly larger than corresponding cirrus amounts from the cloud atlas of WARREN et al. (1986).

2. Ice supersaturation occurs mostly in a broad upper tropospheric layer between 450 and 200 hPa. There is a slight but significant seasonal shift of the altitude distribution of ice-supersaturation layers: the mean altitude is at 300 hPa in summer and fall and descends to 340 hPa in winter and spring.

The frequencies of occurrence of ice supersaturation from the radiosonde data are at 200 hPa in good agreement with the corresponding ISSRs frequencies of occurrence obtained from the MOZAIC data closest to Lindenberg. At 250 hPa there is a large, so far unexplained discrepancy.

The altitude distribution of ice-supersaturation layers over Lindenberg is generally similar to those of subvisible cirrus (from SAGE II data).

3. Ice supersaturation (ISSRs and cirrus clouds) occurs mainly below the tropopause, only a few events extend into the lowermost stratosphere, consistent with the earlier examination of MOZAIC data. Most of the ISSRs and cirrus clouds are situated in a broad layer between the tropopause and 200 hPa below it. Their annual mean pressure distance for the thermal tropopause is -84 ± 58 hPa, the seasonal mean values are -92 ± 58, -59 ± 39, -75 ± 54 and -96 ± 63 hPa for spring, summer, fall and winter, respectively. Similar distributions have been found for cirrus and subvisible cirrus with lidar measurements at the Observatoire de Haute Provence.

4. The vertical extensions of ice-supersaturation layers follows a pair of Weibull distributions with exponent $p = 0.71$ for shallow layers with thickness of less than 1 km and $p \approx 1$ for the thicker ones. The mean thickness of ice-supersaturation layers is 560 m. This value is more similar to the mean thickness of subvisible cirrus than to that of visible cirrus. However, the distribution is rather broad with $\sigma_H = 610$ m. The ice-supersaturation layers of less than 1 km thickness are probably composed of ISSRs, subvisible cirrus, and perhaps thin strata of multi-layer cirrus clouds, whereas the thicker objects are probably mostly cirrus clouds.

5. As in the earlier studies with the MOZAIC and MLS data we determine the distribution of the relative humidity with respect to ice in the upper troposphere. In the subsaturated and the supersaturated range, respectively, the probability of measuring a certain relative humidity decreases exponentially with the relative humidity but with different slopes. While the slope in the subsaturated range is similar to the slope of the distributions found from the MOZAIC data, in the supersaturated range the slope is much steeper than the slopes of the distributions found from the MOZAIC and MLS data.

This is likely the result of the slow response of the RS80A sensor when ascending through cold air. Additionally, there is a bulge in the distribution at about ice saturation, that most probably stems from data obtained in mature cirrus clouds (where the humidity has relaxed to equilibrium and the ice crystals ceased to grow).

For the stratospheric data we find a distribution for the relative humidity with respect to ice that can be fitted by two different exponential distributions for the subsaturated and supersaturated range respectively. Thus, the distribution is quite different from the earlier distributions found from MOZAIC and MLS data, but more similar to the tropospheric distributions (yet without the bulge at saturation). We conjecture that the kink at saturation in the distribution is caused by growing ice crystals in cirrus immediately above the tropopause. The missing bulge at saturation could indicate that these clouds rarely reach an equilibrium state (i.e. the crystals fall out of the supersaturated layer before they completely consume the supersaturation for their growth).

6. The measured temperatures inside the ice-super-

saturation layers are observed to range from −30 and −80 °C; more than 70% of them have temperatures lower than −40 °C, the mean temperature of the ice-supersaturation layers is (-46.8 ± 8.4) °C.

7. Random errors and biases in the humidity measurements do not change the results qualitatively; they only slightly affect the calculated mean values and standard deviations.

In this study we have focused on more general aspects of ice-supersaturation layers but for further studies a more detailed examination of the several ascents could give additional information about the internal structure of these layers. Satellite data could help to make the distinction between cirrus clouds and ISSRs.

Acknowledgements

We thank two anonymous reviewers making useful suggestions that led to a substantial improvement of our manuscript.

References

ANTIKAINEN, V., H. JAUHIAINEN, 1995: Vaisala's new RS90 family of radiosondes. – Vaisala News **136**, 9–12.

ANTIKAINEN, V., A. PAUKKUNEN, 1994: Studies on improving humidity measurements in radiosondes. – WMO Tech. Conf. on Instruments and Methods of Observation, Geneva, Switzerland, WMO Rep. **57**, 137–141.

BERTON, R.P.H., 2000: Statistical distributions of water content and sizes for clouds above Europe. – Ann. Geophysicae **18**, 385–397.

BEYERLE, G., M.R. GROSS, D.A. HANER, N.T. KJOME, I.S. MCDERMID, T.J. MCGEE, J.M. ROSEN, H.-J. SCHÄFER, O. SCHREMS, 2001: A lidar and backscatter sonde measurement campaign at Table Mountain during february–march 1997: Observations of cirrus clouds. – J. Atmos. Sci. **58**, 1275–1287.

DOWLING, D.R., L.F. RADKE, 1990: A summary of physical properties of cirrus clouds. – J. Appl. Meteorol. **29**, 970–978.

DWD, 2000: Witterungsreport Mai 2000, Juli 2000.

ELLIOTT, W.P., D.J. GAFFEN, 1991: On the utility of radiosonde humidity archives for climate studies. – Bull. Amer. Meteor. Soc. **72**, 1507–1520.

GIERENS, K., S. BRINKOP, 2001: A model for the horizontal exchange between ice-supersaturated regions and their surrounding area. – Theor. Appl. Climatol., **71** 129–140.

GIERENS, K., P. SPICHTINGER, 2000: On the size distribution of ice-supersaturated regions in the upper troposphere and the lower stratosphere. – Ann. Geophysicae **18**, 499–504.

GIERENS, K., U. SCHUMANN, M. HELTEN, H. SMIT, A. MARENCO, 1999: A distribution law for relative humidity in the upper troposphere and lower stratosphere derived from three years of MOZAIC measurements. – Ann. Geophysicae **17**, 1218–1226.

GIERENS, K., U. SCHUMANN, M. HELTEN, H. SMIT, P.-H. WANG, 2000: Ice-supersaturated regions and subvisible cirrus in the northern midlatitude upper troposphere. – J. Geophys. Res. **105**, 22743–22753.

GOLDFARB, L., P. KECKHUT, M.-L. CHANIN, A. HAUCHECORNE, 2001: Cirrus climatological results from Lidar Measurements at OHP (44°N, 6°E). – Geophys. Res. Lett. **28**, 1687–1690.

HELTEN, M., H.G.J. SMIT, W. STRÄTER, D. KLEY, P. NEDELEC, M. ZÖGER, R. BUSEN, 1998: Calibration and performance of automatic compact instrumentation for the measurement of relative humidity from passenger aircraft. – J. Geophys. Res. **103**, 25643–25652.

HELTEN, M., H.G.J. SMIT, D. KLEY, J. OVARLEZ, H. SCHLAGER, R. BAUMANN, U. SCHUMANN, P. NEDELEC, A. MARENCO, 1999: In-flight intercomparison of MOZAIC and POLINAT water vapor measurements. – J. Geophys. Res. **104**, 26087–26096.

HEYMSFIELD, A.J., L.M. MILOSHEVICH, 1993: Homogeneous ice nucleation and supercooled liquid water in orographic wave clouds. – J. Atmos. Sci., **50**, 2335–2353.

HEYMSFIELD, A.J., R.M. SABIN, 1989: Cirrus crystal nucleation by homogeneous freezing of solution droplets. – J. Atmos. Sci.,**46**, 2252–2264.

JENSEN, E.J., O.B. TOON, A. TABAZADEH, G.W. SACHSE, B.E. ANDERSON, K.R. CHAN, C.W. TWOHY, B. GANDRUD, S.M. AULENBACH, A. HEYMSFIELD, J. HALLETT, B. GARY, 1998: Ice nucleation processes in upper tropospheric wave–clouds during SUCCESS. – Geophys. Res. Lett. **25**, 1363–1366.

KLEY, D., J.M. RUSSEL III, C. PHILLIPS, (Eds.), 2000: SPARC assessment of upper tropospheric and stratospheric water vapour. WCRP-113, WMO/TD-No. 1043, SPARC Report No. 2., 312 pp. (Available from: SPARC Office, BP 3, F-91371 Verrières le Buisson Cedex, France).

KOOP, T., B. LUO, A. TSIAS, T. PETER, 2000: Water activity as the determinant for homogeneous ice nucleation in aqueous solutions. – Nature **406**, 611–614.

LEITERER, U., H. DIER, T. NAEBERT, 1997: Improvements in radiosonde humidity profiles using RS80/RS90 radiosondes of Vaisala. – Contr. Atmos. Phys. **70**, 319–336.

LEITERER, U., H. DIER, D. NAGEL, T. NAEBERT, D. ALTHAUSEN, K. FRANKE, 2002: Correction method for RS80 A-Humicap humidity profiles. – Internal Report, Meteorological Observatory Lindenberg of Deutscher Wetterdienst, 1–19.

MARENCO, A., V. THOURET, P. NEDELEC, H. SMIT, M. HELTEN, D. KLEY, F. KARCHER, P. SIMON, K. LAW, J. PYLE, G. POSCHMANN, R. VON WREDE, C. HUME, T. COOK, 1998: Measurement of ozone and water vapor by Airbus in-service aircraft: The MOZAIC airborne program, an overview. – J. Geophys. Res. **103**, 25631–25642.

MILOSHEVICH, L.M., H. VÖMEL, A. PAUKKUNEN, A.J. HEYMSFIELD, S.J. OLTMANS, 2001: Characterization and correction of relative humidity measurements from Vaisala RS80-A radiosondes at cold temperatures. – J. Atmos. Oceanic. Technol. **18**, 135–156.

NAGEL, D., U. LEITERER, H. DIER, A. KATS, J. REICHARD, A. BEHRENDT, 2001: High accuracy humidity measurements using the standardized frequency method with a research upper-air sounding system. – Meteorol. Z. **10**, 395–405.

NASH, J., F.J. SCHMIDLIN, 1987: International Radiosonde Intercomparison. Final report. WMO/TD-195, 102 pp.

OVARLEZ, J., P. VAN VELTHOVEN, G. SACHSE, S. VAY, H. SCHLAGER, H. OVARLEZ, 2000: Comparison of water vapor measurements from POLINAT 2 with ECMWF analyses in high humidity conditions. – J. Geophys. Res. **105**, 3737–3744.

OVARLEZ, J., J.-F. GAYET, K. GIERENS, J. STRÖM, H. OVARLEZ, F. AURIOL, R. BUSEN, U. SCHUMANN, 2002: Water vapor measurements inside cirrus clouds in northern and southern hemispheres during INCA. – Geophys. Res. Lett., **29**, 1813.

PAUKKUNEN, A., 1995: Sensor heating to enhance reliability of radiosonde humidity measurement. – Preprints, 9^{th} Symposium on Met. Observ. and Instr., Charlotte, NC, American Meteorological Society, Boston, MA 65–70.

PRUPPACHER, H.R., J.D. KLETT, 1997: Microphysics of Clouds and Precipitation. – Kluwer, Dordrecht, Netherland, 954 pp.

SASSEN, K., 2002: Cirrus clouds – A modern perspective. In: D.K. LYNCH, K. SASSEN, D.O.C. STARR, G. STEPHENS (Eds.): Cirrus. Oxford University press, Oxford, UK, pp. 11–40.

SASSEN, K., B.S. CHO, 1992: Subvisual-thin cirrus lidar dataset for satellite verification and climatological research. – J. Appl. Meteorol. **31**, 1275–1285.

SASSEN, K., G.C. DODD, 1988: Homogeneous nucleation rate for highly supercooled cirrus cloud droplets. – J. Atmos. Sci., **45**, 1357–1369.

SONNTAG,, 1994: Advancements in the field of hygrometry. – Meteorol. Z. **3**, 51–66.

SPANG, R., G. EIDMANN, M. RIESE, D. OFFERMANN, P. PREUSSE, L. PFISTER, P.-H. WANG, 2002: CRISTA observations of cirrus clouds around the tropopause. – J. Geophys. Res. **107**, 8174.

SPICHTINGER, P., K. GIERENS, W. READ, 2002: The statistical distribution law of relative humidity in the global tropopause region. – Meteorol. Z. **11**, No. 2, 83–88.

VAY, S.A., B.E. ANDERSON, E.J. JENSEN, G.W. SACHSE, J. OVALEZ, G.L. GREGORY, S.R. NOLF, J.R. PODOLSKE, T.A. SLATE, C.E. SORENSON, 2000: Tropospheric water vapor measurements over the North Atlantic during the Subsonic Assessment Ozone and Nitrogen Oxide Experiment (SONEX). – J. Geophys. Res. **105**, 3745–3756.

WANG, P.-H., P. MINNIS, M.P. MCCORMICK, G.S. KENT, K.M. SKEENS, 1996: A 6-year climatology of cloud occurrence frequency from Stratospheric Aerosol and Gas Experiment II observations (1985–1990). – J. Geophys. Res. **101**, 29407–29429.

WARREN, S.G., C.J. HAHN, J. LONDON, R.M. CHERVIN, R.L. JENNE, 1986: Global distribution of total cloud cover and cloud type amounts over land. NCAR/TN-273 + STR, available from NTIS, U.S. Department of Commerce, Springfield, Va 22161.

WINKER, D.M., C.R. TREPTE, 1998: Laminar cirrus observed near the tropical tropopause by LITE. – Geophys. Res. Lett. **25**, 3351–3354.